The interplay of the solar wind proton core and halo populations: EMIC instability

S. M. Shaaban,[1,2] M. Lazar,[3,4] S. Poedts,[1] and A. Elhanbaly[2]

Corresponding author: S. M. Shaaban, Centre for Mathematical Plasma Astrophysics, Celestijnenlaan 200B, B-3001 Leuven, Belgium. (shaaban.mohammed@student.kuleuven.be)

[1]Centre for Mathematical Plasma Astrophysics, Celestijnenlaan 200B, B-3001 Leuven, Belgium

[2]Theoretical Physics Research Group, Physics Department, Faculty of Science, Mansoura University, 35516, Egypt

[3]Institut für Theoretische Physik, Lehrstuhl IV: Weltraum- und Astrophysik, Ruhr-Universität Bochum, D-44780 Bochum, Germany

[4]Royal Belgian Institute for Space Aeronomy 3-Avenue Circulaire, B-1180 Brussels, Belgium

Key Points.

- Suprathermal populations in the solar wind.
- The interplay of the core and suprathermal populations.
- Kinetic instabilities: energy transfer between plasma populations.

Abstract.

The kinetic properties of the solar wind protons (ions), like their temperature anisotropy and the resulting instabilities, are in general investigated considering only the proton core (or thermal) populations. The implication of the suprathermal halo components is minimized or just ignored, despite the fact that their presence in the solar wind is continuously reported by the observations, and their kinetic energy density may be significant. Whether they are originating in the corona or solar wind, the energetic particles may result from acceleration by the plasma turbulence, or from the pitch-angle scattering of the streaming protons by the self-generated fluctuations. The presence of suprathermal protons in the heliosphere suggests, therefore, a direct implication in resonant interactions, e.g., Landau, cyclotron, with plasma particles. This paper presents the results of a first investigation on the interplay of the proton core and suprathermal halo, when both these two populations may exhibit temperature anisotropies, which destabilize the electromagnetic ion (proton) cyclotron (EMIC) modes. These results clearly show that, for conditions typically encountered in the solar wind, the effects of the suprathermals can be more important than those driven by the core. Remarkable are also the cumulative effects of the core and halo components, which change dramatically the instability conditions.

1. Introduction

The solar wind plasma particles are not in thermal equilibrium. Measured in situ, the velocity distributions of plasma particles, mainly, electrons and protons, show in general important deviations from a Maxwellian shape, especially determined by the presence of suprathermal populations [Lin, 1998; Lazar et al., 2012a]. Forming the so-called halo components, these populations enhance the high-energy tails of the velocity distributions which are well described by the power-law, or Kappa distribution functions [Vasyliunas, 1968; Christon et al., 1989; Collier et al., 1996; Pierrard and Lazar, 2010].

On the other hand, the solar wind is a hot and dilute plasma, where particle-particle collisions are not efficient to establish the equilibrium. The ubiquitious presence of suprathermal particles confirms this hypothesis, and also suggests the existence of a mechanism of acceleration and energization of plasma particles. There are different physical mechanisms invoked in the particle acceleration, and one of the most efficient interactions occurs by Landau or cyclotron resonances with plasma waves and fluctuations at kinetic electron and ion (proton) scales. These fluctuations are permanently reported by the observations [Jian et al., 2009; Bruno and Carbone, 2013], and may have the origin either in the large-scale perturbations produced by the coronal plasma injections and then transported and decayed in the super-Alfvénic solar wind, or may be enhanced locally by the kinetic instabilities driven by the anisotropy of plasma particles, e.g., the bi-axis temperature anisotropy of the gyrotropic distributions observed in the solar wind and terrestrial magnetosphere (see the review by Marsch [2006] and references therein). In the absence of

collisions it is indubitable that the plasma waves and fluctuations must play a major role triggering the transport of particles and energy in these environments.

A rigorous prediction/description of the wave fluctuations can be achieved by a kinetic treatment of the unstable plasma states and the resulting instabilities using realistic models for the velocity distribution functions (VDFs) of plasma particles. Widely used are the Maxwellian (standard) models [Gary , 1993], which describe well the main (thermal) core of the distribution with different anisotropies, e.g., bi-Maxwellian to describe a (bi-axis) temperature anisotropy, or a drifting-Maxwellian to incorporate streaming components. Standard models were also invoked to describe the suprathermal halo populations [Feldman et al. , 1975; Gary et al., 1996; Maksimovic et al., 2000], **despite the fact that the enhanced suprathermal tails of the distribution are not well-represented without the Kappa power law**.

There is indeed a strong evidence that the entire distribution function can be well adjusted by a superposition of a Maxwellian core, and one or more power-law distributions [Feldman et al., 1973; Marsch et al., 1982; Christon et al., 1991; Sittler Jr. & Burlaga, 1998; Maksimovic et al., 2005; Nieves-Chinchilla & Viñas, 2008]. (A field-aligned strahl may eventually be present as a secondary suprathermal component more pronounced in the energetic events like fast winds or coronal mass ejections). In theoretical predictions the anisotropic Kappa, e.g., bi-Kappa, product-bi-Kappa, are introduced as global models (see the reviews by Hellberg et al. [2005] and Pierrard and Lazar [2010]), incorporating both the core and halo populations in the same global Kappa which is nearly Maxwellian at low energies and decreasing as power-law at high energies. The advantage is that a single (global) Kappa simplifies the approach and implicitly the computations, especially

for the anisotropic models with an increased number of parameters. However, a global Kappa couples unrealistically the core and halo populations describing them with the same parameters, i.e., the same density, temperature and temperature anisotropy, and, **therefore, poorly representing the true distribution and leading to questionable results [Lazar, 2012b]**.

The number of parameters increases considerably if one considers the core and halo as two distinct and anisotropic components, i.e., an anisotropic bi-Maxwellian core (subscript c) with density n_c, and two components of the temperature $T_{c,\parallel}$, $T_{c,\perp}$, **see Eqs. (2–4)** below, and an anisotropic bi-Kappa halo (subscript h) with n_h, two components of the temperature $T_{h,\parallel}$, $T_{h,\perp}$, and the power-index κ to quantify the presence of suprathermal populations, **see Eqs. (5–8)** below. In a recent endeavor to provide a realistic description for the electromagnetic electron cyclotron (EMEC) instability in the solar wind conditions, [Lazar et al., 2014a, 2015a] have shown that such a complex but realistic model is computationally tractable and yields results markedly different than simplified models used before.

Besides the EMEC (or whistler) instability, the electromagnetic ion cyclotron (EMIC) instability plays an equally important role in the solar wind and the subsequent plasma structures, like planetary magnetospheres. Driven by plasma particles with an excess of transverse temperature $T_\perp > T_\parallel$, **these instabilities enhance the electromagnetic fluctuations near the cyclotron frequency**. The same mechanism of cyclotron resonance may also ensure the transfer of energy in opposite direction by dissipating the electromagnetic fluctuations and heating plasma particles. From the entire spectrum of electromagnetic fluctuations decaying in the solar wind [Mangeney et al., 2001; Bruno and

Carbone, 2013], the EMIC waves near the ion (or proton) cyclotron frequency Ω_p, are the first dissipative fluctuations linking two distinct regimes, namely, that of the large scale (fluid) fluctuations of frequency much below Ω_p, and the kinetic regime of high-frequency waves with phase-velocity close to the thermal velocity of plasma particles.

The EMIC instability has been extensively investigated, but the existing studies of the solar wind plasma conditions are limited to simplified models of the VDFs of plasma particles, which facilitate the computations and characterization of the unstable solutions. Thus, early studies have ignored the suprathermal populations, assuming bi-Maxwellian distributed plasmas and providing basic properties of the cyclotron instabilities (see the textbook by Gary [1993] and references therein). The effects of suprathermal protons on the EMIC instability are mainly interpreted using a global bi-Kappa model for the anisotropic protons, see the reviews by Hellberg et al. [2005] and Pierrard and Lazar [2010]. Recently, Lazar [2012b] and Lazar and Poedts [2014b] have shown that these effects are highly dependent on the shape of the distribution by contrasting to a product-bi-Kappa which introduces an excess of free energy and stimulates the instability. More advanced models, which assume two distinct components, namely, a core and a halo, were also considered, but with limitations, either minimizing the effects of suprathermals by considering both the core and halo populations bi-Maxwellian distributed [Gary et al., 1996], or neglecting completely thermal effects of the core by considering this component cold, i.e., $T_c \to 0$ [Xiao et al., 2007].

In this paper we propose a new approach of the EMIC instability on the basis of a realistic kinetic model of the proton VDF, which combines a bi-Maxwellian core and a bi-Kappa halo populations. This new approach enables us to study for the first time

the interplay of the thermal core and suprathermal halo, especially when both these two components are anisotropic. Our study is focused on the solar wind conditions which destabilize the EMIC modes. The paper is organized as follows: In section 2 we introduce the velocity distribution models for the proton populations. The electrons are assumed isotropic, allowing us to isolate the effects of protons, and quantify the individual contributions of the proton core and halo components. In section 3 we derive the dispersion relation for the EMIC modes and analyze the threshold conditions and unstable solutions by contrast to those provided before with simplified models. The results of the present study are summarized and discussed in section 4.

2. Dual Core-Halo Distributions

In the absence of strahl or beaming components, there is no relative drift between suprathermal and core populations. The velocity distribution functions measured in-situ are gyrotropic, and present a dual structure, namely, with a core (subscript c) and a halo (subscript h), for any sort of plasma particle (subscript $\alpha = e, p$ for electrons and protons, respectively)

$$F_\alpha\left(v_\parallel, v_\perp\right) = F_{\alpha,c}\left(v_\parallel, v_\perp\right) + F_{\alpha,h}\left(v_\parallel, v_\perp\right). \tag{1}$$

Each of these two components can exhibit a temperature anisotropy $A = T_\perp/T_\parallel \neq 1$ with respect to the uniform magnetic field. The core population is described by the unperturbed bi-Maxwellian distribution

$$F_{\alpha,c}\left(v_\parallel, v_\perp\right) = \frac{1}{\pi^{3/2} u_{\alpha,\perp}^2 u_{\alpha,\parallel}} \exp\left(-\frac{v_\parallel^2}{u_{\alpha,\parallel}^2} - \frac{v_\perp^2}{u_{\alpha,\perp}^2}\right), \tag{2}$$

with thermal velocities $u_{\alpha,\parallel,\perp}$ defined by

$$T_{c,\parallel}^M = \frac{m_\alpha}{k_B} \int d\mathbf{v} v_\parallel^2 F_\alpha(v_\parallel, v_\perp) = \frac{m_\alpha u_{\alpha,\parallel}^2}{2k_B} \tag{3}$$

$$T^M_{c,\perp} = \frac{m_\alpha}{2k_B}\int d\mathbf{v} v^2_\perp F_\alpha(v_\parallel, v_\perp) = \frac{m_\alpha u^2_{\alpha,\perp}}{2k_B}. \quad (4)$$

The suprathermal (halo) tails are described by a bi-Kappa VDF [Summers and Thorne , 1991]

$$F_{\alpha,h} = \frac{1}{\pi^{3/2}\theta^2_{\alpha,\perp}\theta_{\alpha,\parallel}}\frac{\Gamma(\kappa+1)}{\Gamma(\kappa-1/2)}\left[1+\frac{v^2_\parallel}{\kappa\theta^2_{\alpha,\parallel}}+\frac{v^2_\perp}{\kappa\theta^2_{\alpha,\perp}}\right]^{-\kappa-1}. \quad (5)$$

This distribution function is normalized to unity $\int d^3v F_\alpha = 1$, and is writen in terms of the generalized thermal velocities $\theta_{\alpha,\parallel,\perp}$, which are defined, for a power-index $\kappa > 3/2$, by

$$T^K_{h,\parallel} = \frac{2\kappa}{2\kappa-3}\frac{m_\alpha\theta^2_{\alpha,\parallel}}{2k_B}, \quad T^K_{h,\perp} = \frac{2\kappa}{2\kappa-3}\frac{m_\alpha\theta^2_{\alpha,\perp}}{2k_B}. \quad (6)$$

The halo temperature is increased with increasing the suprathermal populations [Lazar et al., 2015b], which are quantified by a finite power-index κ,

$$T^K_{h,\parallel,\perp} = \frac{2\kappa}{2\kappa-3}T^M_{h,\parallel,\perp} > T^M_{h,\parallel,\perp}. \quad (7)$$

Implicitly, the plasma beta parameter $\beta = 8\pi n k_B T/B^2_0$ can be defined for each of the core and halo populations, and their parallel components used in our calculations read

$$\beta^M_{c,\parallel} = \frac{8\pi n_c k_B T^M_{c,\parallel}}{B^2_0}, \quad \beta^K_{h,\parallel} = \frac{8\pi n_h k_B T^K_{h,\parallel}}{B^2_0} = \frac{2\kappa}{2\kappa-3}\beta^M_{h,\parallel} > \beta^M_{h,\parallel}, \quad (8)$$

Such a dual structure has been reported for both major species of space plasma particles, e.g., by Feldman et al. [1973]; Marsch et al. [1982]; Christon et al. [1991] for protons, and by Vasyliunas [1968]; Feldman et al. [1975]; Maksimovic et al. [1997]; Pierrard et al. [1999]; Maksimovic et al. [2005] for electrons. In the present approach the electrons will be taken isotropic and sufficiently cold since our intention is to isolate and describe only the effects of the anisotropic protons on the instability of the EMIC modes.

3. Stability Analysis: EMIC Modes

We restrain to parallel modes since in the direction parallel to the stationary magnetic field $\boldsymbol{B_0}$, the EMIC instability is decoupled from the electrostatic modes and exhibits maximum growth rates [Kennel and Petschek, 1966]. For a collisionless and homogenous plasma of electrons and protons described by the core and halo distributions (2)–(8), the dispersion relations for the parallel electromagnetic modes read

$$\begin{aligned}\frac{c^2k^2}{\omega^2} = 1 \quad &+ \sum_{\alpha=e,p} \frac{\omega_{\alpha,c}^2}{\omega^2} \left[\frac{\omega}{ku_{\alpha,\|}} Z\left(\xi_\alpha^\pm\right) + \left(A_{\alpha,c}-1\right)\left\{1+\xi_\alpha^\pm Z\left(\xi_\alpha^\pm\right)\right\}\right] \\ &+ \sum_{\alpha=e,p} \frac{\omega_{\alpha,h}^2}{\omega^2} \left[\frac{\omega}{k\theta_{\alpha,\|}} Z_\kappa\left(g_\alpha^\pm\right) + \left(A_{\alpha,h}-1\right)\left\{1+g_\alpha^\pm Z_\kappa\left(g_\alpha^\pm\right)\right\}\right], \end{aligned} \tag{9}$$

where ω is the wave-frequency, k is the wave-number, c is the light speed, $\omega_{\alpha,c,h}^2 = 4\pi n_{c,h}e^2/m_\alpha$ are the plasma frequencies of the core (subscript c) and halo (subscript h), $A_{\alpha,c,h} = \left(T_{\alpha,\perp}/T_{\alpha,\|}\right)_{c,h}$ are the temperature anisotropies, $\pm$ denote the circular polarizations, right-handed (RH) and left-handed (LH), respectively,. The dispersion relations are derived in terms of the plasma dispersion function [Fried and Conte , 1961]

$$Z\left(\xi_\alpha^\pm\right) = \frac{1}{\pi^{1/2}} \int_{-\infty}^{\infty} \frac{\exp\left(-x^2\right)}{x-\xi_\alpha^\pm} dt, \quad \Im\left(\xi_\alpha^\pm\right) > 0, \tag{10}$$

of argument

$$\xi_\alpha^\pm = \frac{\omega \pm \Omega_\alpha}{ku_{\alpha,\|,}}, \tag{11}$$

and the modified (Kappa) dispersion function [Lazar et al., 2008]

$$Z_\kappa\left(g_\alpha^\pm\right) = \frac{1}{\pi^{1/2}\kappa^{1/2}} \frac{\Gamma\left(\kappa\right)}{\Gamma\left(\kappa-1/2\right)} \int_{-\infty}^{\infty} \frac{\left(1+x^2/\kappa\right)^{-\kappa}}{x-g_\alpha^\pm} dx, \quad \Im\left(g_\alpha^\pm\right) > 0, \tag{12}$$

of argument

$$g_\alpha^\pm = \frac{\omega \pm \Omega_\alpha}{k\theta_{\alpha,\|}}. \tag{13}$$

where $\Omega_\alpha = q_\alpha \boldsymbol{B}_0/m_\alpha c$ is the gyrofrequency (nonrelativistic).

If we neglect thermal effects of electrons, keeping only the zero-order term in the large argument ($|\xi_e|^+ \gg 1$) approximation of their dispersion function, the dispersion relation (9) for the EMIC modes (subluminal, $\omega^2 \ll k^2c^2$) with $\omega < \Omega_p \ll |\Omega_e|$ can be rewritten with normalized quantities as follows

$$\tilde{k}^2 = A_h - 1 + \frac{A_h(\tilde{\omega}-1)+1}{\tilde{k}\sqrt{\beta^M_{h,\parallel}}} Z_\kappa\left(\frac{\tilde{\omega}-1}{\tilde{k}\sqrt{\beta^M_{h,\parallel}}}\right) - \tilde{\omega} + \frac{1}{\eta}\left[A_c - 1 + \frac{A_c(\tilde{\omega}-1)+1}{\tilde{k}\sqrt{\eta\beta^M_{c,\parallel}}} \times Z\left(\frac{\tilde{\omega}-1}{\tilde{k}\sqrt{\eta\beta^M_{c,\parallel}}}\right) - \tilde{\omega}\right], \quad (14)$$

where $\tilde{\omega} = \omega/\Omega_p$, $\tilde{k} = kc/\omega_{p,h}$, $\beta^M_{c,\parallel} = 8\pi n_c k_B T^M_{c,\parallel}/B_0^2$ and $\beta^M_{h,\parallel} = 8\pi n_h k_B T^M_{h,\parallel}/B_0^2$ are the parallel proton beta parameter for the core and halo, respectively, and $\eta = n_h/n_c$ is the halo–core relative density.

The core may be less anisotropic than the halo, and if we take the core isotropic $A_c = 1$, the dispersion relation (14) reduces to

$$\tilde{k}^2 = A_h - 1 + \frac{A_h(\tilde{\omega}-1)+1}{\tilde{k}\sqrt{\beta^M_{h,\parallel}}} Z_\kappa\left(\frac{\tilde{\omega}-1}{\tilde{k}\sqrt{\beta^M_{h,\parallel}}}\right) + \frac{\tilde{\omega}}{\eta^{1.5}\tilde{k}\sqrt{\beta^M_{c,\parallel}}} Z\left(\frac{\tilde{\omega}-1}{\tilde{k}\sqrt{\eta\beta^M_{c,\parallel}}}\right) - \tilde{\omega} - \frac{\tilde{\omega}}{\eta}. \quad (15)$$

Moreover, if the core is cold enough, i.e., $T_c \to 0$, a situation however unrealistic for the solar wind, we may consider the zero-order approximation of the plasma dispersion function in the limit of very large arguments $Z(|\xi| \gg 1) = -\xi^{-1}$, and recover the dispersion relation derived by Xiao et al. [2007]

$$\tilde{k}^2 = A_h - 1 + \frac{A_h(\tilde{\omega}-1)+1}{\tilde{k}\sqrt{\beta^M_{h,\parallel}}} Z_\kappa\left(\frac{\tilde{\omega}-1}{\tilde{k}\sqrt{\beta^M_{h,\parallel}}}\right) - \frac{\tilde{\omega}}{\eta(\tilde{\omega}-1)} - \frac{\tilde{\omega}(\eta+1)}{\eta}. \quad (16)$$

3.1. *The unstable solutions*

In this section, we discuss the EMIC unstable solutions and identify the most relevant cases determined by the interplay of the core and halo populations and their influence

on the growth rates, wave-frequency and the unstable wave-numbers. The main distinct conditions analyzed here are determined by the plasma parameters which characterize these two populations in the solar wind. The existing observational data provide representative (mean or limit) values making a distinct characterization of the core and halo populations only for the solar wind electrons, while the proton data are limited to the core component. To characterize the proton halo we invoke values deduced indirectly from the electrons and other complementary data. Thus, two representative values of the halo–core density ratio, $\eta = 0.01$ and 0.05 found relevant for the solar wind electrons, are also adopted here for protons on the basis of charge neutrality condition. For the proton core, values of the temperature anisotropy A_c and parallel plasma beta $\beta_{c,\|}$ are extracted from the histograms built by Kasper et al. [2003] with 1.6 million observations in slow winds ($V_{\rm SW} < 400$ km/s) collected by Wind during a long interval of time between 1994 and 2001. The proton core concentrates to states of energy equipartition $\beta_c \simeq 1$ with a moderate temperature anisotropy (driving EMIC modes), usually satisfying $A_c < 2$. Spectral characteristic of the suprathermal populations are in general similar for both electrons and protons [Christon et al., 1989], although for ions, the most probably values of the power-index κ are in general higher than those found for electrons [Collier et al., 1996]. More tenous than the core, the suprathermal halo may also be more anisotropic and expected to concentrate at lower values of the plasma beta parameter $\beta_{h,\|} < \beta_{c,\|}$.

Figures 1 and 2 present the unstable EMIC solutions, the growth rates and wave-frequencies, respectively, providing a suggestive comparison between the realistic approach proposed in the present paper and the simplified approaches considered before, e.g., a cold core plus a bi-Kappa halo [Xiao et al., 2007], two-Maxwellian models [Gary et al., 1996].

If the core is considered cold ($T_c \to 0$, an assumption completely unrealistic for the solar wind), all the EMIC mode features, namely, growth-rates, wave-frequencies and wave-numbers are significantly overestimated. Otherwise, the instability driven by the halo anisotropy ($A_h > 1$) is inhibited by a finite thermal spread in the core, see the case with isotropic core. An additional anisotropy of the core $A_c > 1$ may considerably enhance the instability, increasing the growth-rates, the range of unstable wave-numbers and the wave frequencies. When both the halo and core components are anisotropic, two peaks of the growth rates may become visible, the first at lower wave-numbers is driven by the anisotropic halo, while the second peak is driven by the anisotropic core. The second peak becomes apparent and may exceed the halo peak only when the influence (or the presence) of the suprathermals, quantified in this case by two parameters η and κ, is diminished, i.e., for lower values of the halo-core relative density, e.g., $\eta = 0.01$, and high values of the power-index, e.g., $\kappa = 6, \infty$. As expected, the difference between these peaks becomes less important in the limit of a Maxwellian halo ($\kappa \to \infty$). If we increase the presence of suprathermals by increasing the halo-core relative density to $\eta = 0.05$, the growth rates restrain to low wave-numbers and exhibit only one peak driven by the suprathermal halo. The EMIC wave-frequency is not much sensitive to the power-index κ, but the growth rates are in general stimulated and the unstable wave-numbers extend to markedly lower values with a decrease of this parameter.

We can already notice that suprathermals may have an important destabilizing effect on the EMIC modes, and in many situations this effect appears to be more significant than that produced by the core. Therefore, in the next three figures, Figs. 3–5, we describe in detail the influence of the halo parameters, i.e., A_h, $\beta_{h,\parallel}$ and η, on the EMIC instability.

This influence may however be highly dependent on the core properties, as shown already in Figures 1 and 2, and for that reason we keep in the next comparative analysis all the three models for the core, i.e., cold, isotropic and anisotropic. Figure 3 show a monotonic increase of the (maximum) growth rates with the increase of anisotropy $A_h = 1.5, 2, 2.5$, or the increase of parallel plasma beta $\beta_h^M = 0.1, 0.5, 1$. The second peak stimulated by the anisotropic core, see panels (c), remains dominated by the first peak driven by the more anisotropic halo.

The results presented in Figs. 1 and 2 suggest that the halo-core density ratio η may play as a key factor in stimulating or suppressing the growth rates. In Figures 4 and 5 we examine the effect of the halo-core density ratio by taking two representative values $\eta = 0.05$ and 0.01. The EMIC solutions displayed in Figure 4, including both the growth rate and the wave-frequency, are derived for maximum growth rates in the vicinity of $\gamma_m = 10^{-2}\Omega_p$. The same three models are considered for the core, and the unstable solutions are obtained for $\beta_h^M = 0.5$, $A_h = 1.5$, $\beta_c^M = 1$, and $\kappa = 6$. In all these cases the growth rates and the wave-frequencies are enhanced by increasing the relative density of halo population from $\eta = 0.01$ to 0.05. However the range of **unstable** wave-numbers is considerably reduced by the same increase of η. The growth rate shows a second peak when the core-anisotropy is large enough and comparable to the halo-anisotropy, i.e., $A_c = 1.45$. In Figure 5 we extend this examination for the same plasma parameters as in Figure 4, but for a lower anisotropy $A_h = 1.15$ yielding unstable solutions with lower values of the maximum growth-rate in the vicinity of $\gamma_m = 10^{-3}\Omega_p$. In this case the increase of relative density η has an opposite influence, lowering the growth rates, the range of unstable wave-numbers and wave-frequencies. If appears, the core peak is

again dominated by the halo peak, although the core anisotropy $A_c = 1.45$ is (maybe unrealistically) higher than the halo anisotropy.

In Figure 6 we show the effect of the core anisotropy $A_c = 1, 1.5, 2$ on the EMIC instability mainly driven the anisotropic halo anisotropy with $A_h = 2.5$, $\beta_h^M = 0.05$, $\eta = 0.05$, and different power-index $\kappa = 3, 6, \infty$. Both the growth rate and the wave-frequency are enhanced by increasing the core anisotropy and **this effect is stimulated by the suprathermals, by decreasing the power-index** κ. The EMIC modes are stable (damped modes) for a two-Maxwellian model ($\kappa \to \infty$) with an isotropic core ($A_c = 1$), a case studied by Gary et al. [1994], but the instability develops for lower values of $\kappa = 6$, 3. Moreover, the relative halo population is high enough $\eta = 0.05$, preventing the growth rates to develop a second peak.

Now we have to remember that our present analysis assumes a Kappa distributed halo with κ-dependent temperature, see section 2. There is also an alternative method widely used in the investigations of suprathermal populations -modeled with the same Kappa distribution functions but with κ-independent temperature. However, according to recent studies [Lazar et al., 2015b, 2016], a Kappa distributed halo with κ-dependent temperature enables a more realistic interpretation of the suprathermal populations and their effects, e.g., on the kinetic instabilities. Figure 7 provides a comparative characterization of the EMIC solutions obtained with these two Kappa approaches. The left panels display the EMIC growth-rates obtained for the Kappa model used in this work, i.e., with $T^K_{h,\parallel,\perp} > T^M_{h,\parallel,\perp}$. These growth-rates show a systematic enhancement with the decrease of κ-index, which seems to confirm the expectation that kinetic instabilities may be stimulated by the excess of free energy of the suprathermals. In the right panels we display the

growth-rates derived for the same plasma parameters but using a Kappa approach with $T^K_{h,\parallel,\perp} = T^M_{h,\parallel,\perp}$. In this case it becomes complicated to decode the effect of suprathermal populations quantified by the power-index κ. Lazar et al. [2015b] have already noticed that, contrary to the expectations, these cyclotron instabilities of the EMIC or EMEC modes, are in general inhibited for lower values of κ. Only the very small growth rates close to the marginal stability ($\gamma \to 0$) are enhanced by the suprathermals. **Such a non-uniform influence of the suprathermals can be recognized in Figure 7. Thus, the growth-rates obtained for a cold core (top panel) are stimulated at low wave-numbers, but their peaks obtained at higher wave-numbers are considerably inhibited by lowering the power-index κ. For a core with a finite thermal spread, the influence of suprathermals is opposite, especially that shown by the peaks obtained for an isotropic core (middle panel), while for an anisotropic core this influence seems to be again function of the wave-number value (bottom panel).**

3.2. *The instability thresholds*

In Figures 8 and 9 we display the instability tresholds as isocontours of the maximum growth rates at two distinct levels, $\gamma_m/\Omega_p = 10^{-3}$, and 10^{-2}, the lower one approaching the marginal stability of the EMIC modes. These thresholds provide a more comprehensive picture for the properties of the EMIC instability under the interplay of the core and suprathermal populations, for extended conditions satisfied by the suprathermal halo populations in the solar wind and planetary magnetospheres, e.g., $0.01 < \beta_{h,\parallel} < 10$. The comparative analysis include the effects of the halo-core density ratio η in Figure 8 and the power-index κ in Figure 9 and make a clear distinction between the same three models

considered above for the core, namely, cold core ($T_c \to 0$), isotropic $A_c = 1$, or anisotropic with $A_c > 1$. The EMIC thresholds are obtained with an inverse correlation law between the temperature anisotropy A_h and the parallel plasma beta $\beta^M_{h,\parallel}$

$$A_h = \left(1 + \frac{a}{{\beta^M_{h,\parallel}}^b}\right) \frac{c}{{\beta^M_{h,\parallel}}^d}, \tag{17}$$

where the values of the fitting parameters a, b, c, and d are provided in Tables 1 and 2. The classical case of the inverse correlation law introduced by Gary and Lee [1994] is recovered as for particular values of $c = 1$ and $d = 0$.

The effect of the halo-core density ratio η on the instability thresholds in Figure 8 is not uniform, being highly dependent of $\beta^M_{h,\parallel}$ and A_h. A more dense halo is expected to lower the instability thresholds and this is effect is indeed confirmed for sufficiently large values of $\beta^M_{h,\parallel} > 0.1$. For lower values of $\beta^M_{h,\parallel} < 0.1$ the kinetic effects are dominated by the core, and the instability thresholds conditioned by the halo component increase considerably. The instability thresholds are also lowered by the suprathermal populations quantified by the power-index κ in Figure 9. This effect is again more significant for lower values of $\beta^M_{h,\parallel} < 0.1$, when the main free energy of the halo component resides in the suprathermal tails and not in the thermal spread of this component. Naturally, the influence of suprathermals diminishes with decreasing the relative halo-core density (right panels). The instability thresholds confirm the effects of η and κ parameters on the growth-rates found in the particular cases from section 3.1. In the cold-core limit the growth-rates are overestimated but the instability thresholds are, implicitly, underestimated.

4. Concluding Discussions

We have refined the linear kinetic approach of the EMIC instability on the basis of an advanced modelling of the proton velocity distribution in accord with the observations in the solar wind. The low-frequency fluctuations detected in the solar wind may be enhanced locally by this instability driven by the anisotropic protons. Moreover, in the absence of energetic events the in-situ measurements reveal a dual structure of the velocity distributions of plasma particles, with a thermal (Maxwellian) core and a suprathermal (Kappa) halo. Each of these two components can exhibit temperature anisotropy and implicitly drive instabilities of the EMIC modes. Many studies of this instability that claim applicability in the solar wind, are in general based on simplified models of the velocity distributions, minimizing or just ignoring effects of suprathermal populations. In the present paper we have shown that a realistic approach of this instability in the solar wind conditions must take into account the suprathermal protons, which may significantly change the instability conditions.

The EMIC unstable solutions analyzed in section 3 are derived for plasma parameters typically encountered in the solar wind. These solutions are provided not only for the realistic approach proposed in the present paper, but for a number of simplified models considered before, e.g., a cold core plus a bi-Kappa (or bi-Maxwellian) halo, or two-Maxwellian models, enabling us to make a comparative analysis and outline the interplay of the core and halo populations and their influence on the growth rates, wave-frequency and the unstable wave-numbers. Thus, the main properties of the EMIC instability, namely, growth-rates, wave-frequencies and wave-numbers are markedly overestimated when the core is considered cold ($T_c \to 0$), an assumption completely unrealistic for the

solar wind. Otherwise, the instability driven by the halo anisotropy $A_h > 1$ is inhibited by a finite thermal spread in the core, but can be stimulated by the anisotropy of the proton core $A_c > 1$. The growth rates may therefore show a second distinct peak of the unstable EMIC modes driven by the anisotropic core at larger wave-numbers. The occurrence of the core peak is directly conditioned by an increase of the core population (i.e., relative to the halo by decreasing η), and an enhancement of the core anisotropy. Growth-rates with two peaks are also obtained for a two-Maxwellian approach, i.e., Maxwellian core plus Maxwellian halo ($\kappa \to \infty$), but here we have shown that the halo peak is significantly enhanced by the suprathermal populations quantified by the low values of κ-index. In addition, the effect of the halo-core relative density η on the growth rate, real frequency, and the instability thresholds is found to be dependent on the halo temperature anisotropy and the plasma beta parameter of this component. **A series of punctual conclusions that are evident from Figures 1 through 9 may be itemized as follows: (a) Growth rates increase with decreasing κ (i.e. broader suprathermal distribution). (b) Growth rates increase with increasing suprathermal anisotropy. (c) Growth rates increase with increasing core anisotropy. (d) Growth rates increase with increasing suprathermal beta. (e) When suprathermal anisotropy is high, growth rates increase with increasing suprathermal/core relative abundance. (f) When suprathermal anisotropy is low, growth rates decrease with increasing suprathermal/core relative abundance. (g) A higher suprathermal fraction requires a higher suprathermal anisotropy to reach an instability threshold. (h) A lower κ requires a lower (halo) anisotropy to reach an instability threshold.**

It becomes clear that the presence of suprathermal populations in conditions specific to the solar wind and planetary magnetosphere has an important impact on the EMIC instability. We have found an significant contrast between the instability conditions resulted from the interplay of the core and halo populations and those predicted by simplified models which neglect either the presence of suprathermal populations or the thermal spread of the core. By this, the results of the present paper demonstrate that the existing interpretations of this instability, especially the instability conditions and the role played by the EMIC modes in key processes in space plasmas must reconsidered. An important aspect that we plan to re-evaluate in the future studies is the energy transfer mediated by these instabilities between suprathermal and thermal components.

Acknowledgments. The authors acknowledge support from the Katholieke Universiteit Leuven, the Ruhr-University Bochum, and Alexander von Humboldt Foundation. These results were obtained in the framework of the projects GOA/2015-014 (KU Leuven), G0A2316N (FWO-Vlaanderen), and C 90347 (ESA Prodex 9). The research leading to these results has also received funding from IAP P7/08 CHARM (Belspo), and the European Commission's Seventh Framework Programme FP7-PEOPLE- 2010-IRSES-269299 project-SOLSPANET(www.solspanet.eu). S. M. Shaaban would like to thank the Egyptian Ministry of Higher Education for supporting his research activities.

References

Bruno, R., and V. Carbone (2013), The solar wind as a turbulence laboratory, *Living Rev. Solar Phys.,* 10, 2.

Christon, S.P., D.J. Williams, (1989) Mitchell, D.G., Frank, L.A., Huang, C.Y., Spectral characteristics of plasma sheet ion and electron populations during undisturbed geomagnetic conditions, *J. Geophys. Res.,* 94, 13409.

Christon, S.P., D.J. Williams, D.G. Mitchell, C.Y. Huang, L.A. Frank (1991), Spectral characteristics of plasma sheet ion and electron populations during disturbed geomagnetic conditions, *J. Geophys. Res.,* 96, 1.

Collier, M.R., D.C. Hamilton, G. Gloeckler, P. Bochsler, R.B. Sheldon (1996), Neon-20, Oxigen-16, and Helium-4 densities, temperatures, and supraathermal tails in the solar wind determined with WIND/MASS, *Geophys. Res. Lett.,* 23, 1191.

Feldman, W. C., J. R. Asbridge, S. J. Bame, and M. D. Montgomery (1973), Double ion streams in the solar wind, *J. Geophys. Res.,* 78, 2017.

Feldman, W. C., J. R. Asbridge, S. J. Bame, M. D. Montgomery, and S. P. Gary (1975) Solar wind electrons, *J. Geophys. Res.,* , 80, 4181.

Fried, B. D., and S. D. Conte (1961), *The Plasma Dispersion Function*, Academic Press, New York.

Gary, S. P. (1993), *Theory of space plasma microinstabilities*, Cambridge university press.

Gary, S. P., and M. A. Lee (1994), The ion cyclotron anisotropy instability and the inverse correlation between proton anisotropy and proton beta, *J. Geophys. Res.,* 99, 11297.

Gary, S.P., M.B. Moldwin, M.F. Thomsen, D. Winske D.J. McComas (1994), Hot proton anisotropies and cool proton proton temperatures in the outer magnetosphere, *J. Geophys. Res.,* 99, 23,603.

Gary, S.P., V.M. Vazquez, D. Winske (1996), Electromagnetic proton cyclotron instability: Proton velocity distributions, *J. Geophys. Res.,* 101, 13327.

Hellberg, M., R. Mace, T. Cattaert (2005), Effects of superthermal particles on waves in magnetized space plasmas, *Space Sci. Rev.,* 121, 127.

Jian, L.K., C.T. Russell, J.G. Luhmann, R.J. Strangeway, J.S. Leisner, A.B. Galvin (2009), Ion cyclotron waves in the solar wind observed by stereo near 1 AU, *Astrophys. J.,* 701, L105.

Kennel, C. F., and H. E. Petschek (1966), Limit on stably trapped particle fluxes, *J. Geophys. Res.,* 71, 1.

Kasper, J. C., A. J. Lazarus, S. P. Gary, and A. Szabo (2003), Solar wind temperature anisotropies, in Solar Wind Ten, edited by M. Velli, R. Bruno, and F. Malara, AIP Conf. Proc., 679, 538541.

Lazar, M., R. Schlickeiser, and P. K. Shukla (2008), Cumulative effect of the Weibel-type instabilities in symmetric counterstreaming plasmas with kappa anisotropies, *Phys. Plasmas,* 15, 042103.

Lazar, M., R. Schlickeiser, and S. Poedts (2012a), in Exploring the Solar Wind, (InTech, Ed. M. Lazar), 241, available from: http://www.intechopen.com/books/exploring-the-solar-wind/

Lazar, M. (2012b), The electromagnetic ion-cyclotron instability in bi-Kappa distributed plasmas, *Astron. Astrophys.,* 547, A94.

Lazar, M., S. Poedts (2014b), Instability of the parallel electromagnetic modes in Kappa distributed plasmas II. Electromagnetic ioncyclotron modes, *Mon. Not. R. Astron. Soc.,* , 437, 641.

Lazar, M., S. Poedts, and R. Schlickeiser (2014a), The interplay of Kappa and core populations in the solar wind: Electromagnetic electron cyclotron instability, *J. Geophys. Res.,* 119, 9395.

Lazar, M., S. Poedts, S., R. Schlickeiser, C. Dumitrache (2015a), Towards realistic parametrization of the kinetic anisotropy and the resulting instabilities in space plasmas. Electromagnetic electroncyclotron instability in the solar wind, *Mon. Not. R. Astron. Soc.,* 446, 3022.

Lazar, M., S. Poedts, and H. Fichtner (2015b), Destabilizing effects of the suprathermal populations in the solar wind, *Astron. Astrophys.,* 582, A124.

Lazar, M., H. Fichtner, and P.H. Yoon (2016), On the interpretation and applicability of -distributions, *Astron. Astrophys.,* (2016), submitted.

Lin, R.P. (1998), Wind observations of suprathermal electrons in the interplanetary medium, *Space Sci. Rev.,* 86, 61.

Maksimovic, M., V. Pierrard, and P. Riley (1997), Ulysses electron distributions fitted with Kappa functions, *Geophys. Res. Lett.,* 24, 1151.

Maksimovic, M., S.P. Gary, R.M. Skoug (2000), Solar wind electron suprathermal strength and temperature gradients: Ulysses observations, *J. Geophys. Res.,* **105, 18337.**

Maksimovic, M., I. Zouganelis, J. Y. Chaufray, K. Issautier, E. E. Scime, J. E. Littleton, et al., (2005), Radial evolution of the electron distribution functions in the fast solar wind between 0.3 and 1.5 AU., *J. Geophys. Res.,* 110, A09104.

Mangeney, A., C. Salem, P. Veltri, C. Cecconi (2001), Intermittency in the solar wind turbulence and the Haar wavelet transform, in: Sheffield Space Plasma Meeting: Multipoint Measurements versus Theory, edited by: Warmbein, B., vol. 492 of ESA Special Publication, 53 pp.

Marsch, E. (2006), Kinetic physics of the solar corona and solar wind, *Living Rev. Solar Phys.*, 3, 1. http://www.livingreviews.org/lrsp-2006-1

Marsch, E., K-H. Mühlhäuser, R. Schwenn, H. Rosenbauer, W. Pilipp, and F. M. Neubauer (1982), Solar wind protons: Threedimensional velocity distributions and derived plasma parameters measured between 0.3 and 1 AU, *J. Geophys. Res.,* 87, 52.

Nieves-Chinchilla, T., A.F. Viñas (2008), Solar wind electron distribution functions inside magnetic clouds, *J. Geophys. Res.,* 113, A02105.

Pierrard, V., M. Maksimovic, and J. Lemaire (1999), Electron velocity distribution functions from the solar wind to the corona, *J. Geophys. Res.,* 104, 17021.

Pierrard, V., and M. Lazar. (2010), Kappa distributions: Theory and applications in space plasmas, *Solar Phys.* 267, 153.

Sittler Jr., E.C., L.F. Burlaga (1998), Electron temperatures within magnetic clouds between 2 and 4 AU: Voyager 2 observations, *J. Geophys. Res.,* 103, 17447.

Summers, D., and R. M. Thorne (1991), The modified plasma dispersion function, *Phys. Plasmas,* 3, 1835.

Vasyliunas, V.M., (1968), A survey of low-energy electrons in the evening sector of the magnetosphere with OGO 1 and OGO 3, *J. Geophys. Res.,* 73, 2839.

Xiao, F., Q. Zhou, H. He, H. Zheng, and S. Wang (2007), Electromagnetic ion cyclotron waves instability threshold condition of suprathermal protons by kappa distribution, *J. Geophys. Res.,* 112, A07219.

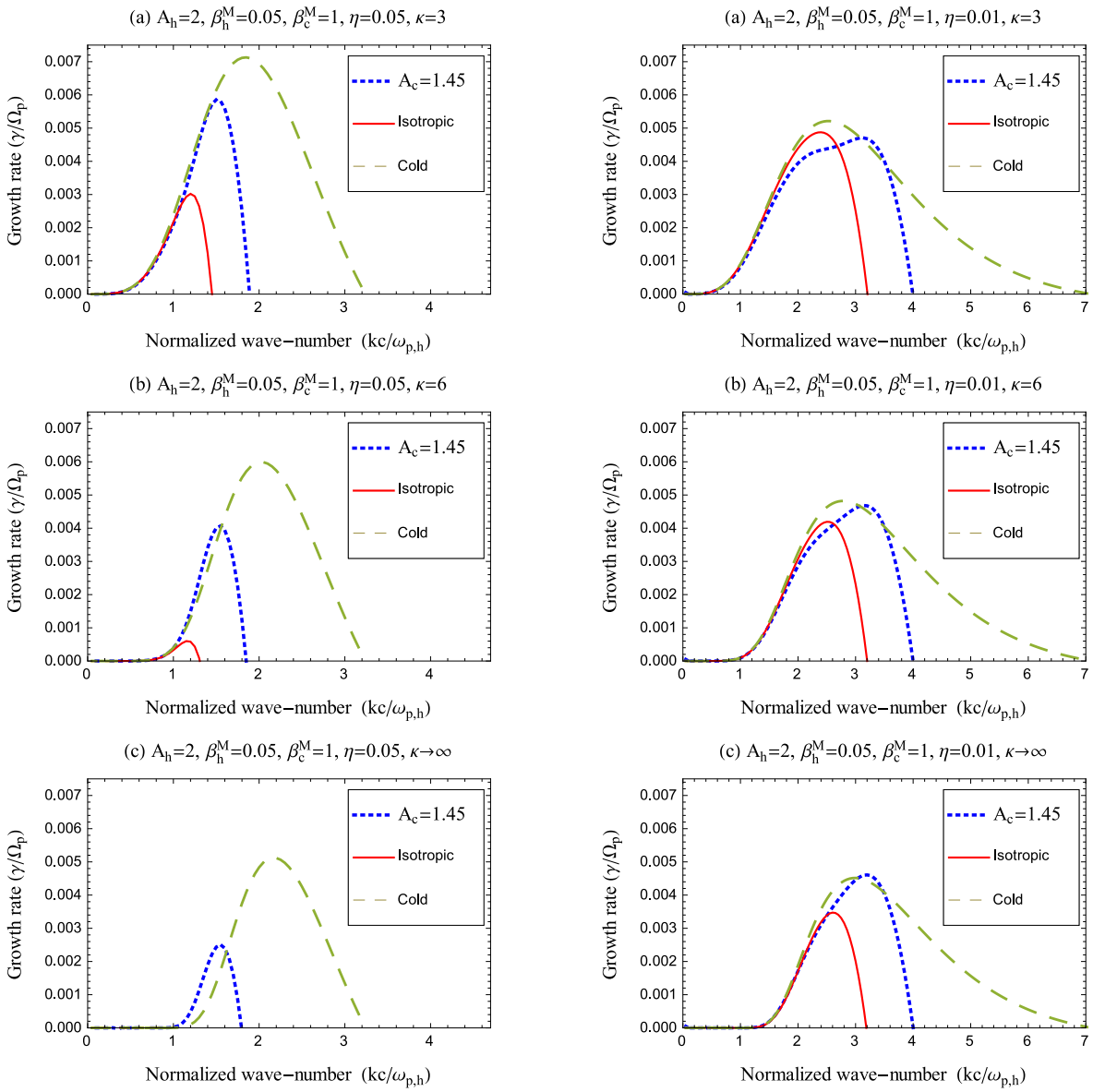

Figure 1. Comparison between the growth rates of the EMIC instability obtained with three distinct models for the core: cold (dashed lines), isotropic (solid lines), and anisotropic with $A_c = 1.45$ (dotted lines), two density ratios $\eta = 0.05$ (left), and $\eta = 0.01$ (right), and different power-indices $\kappa = 3$ (top), 6 (middle), and ∞ (bottom). The other parameters are $A_h = 2$, $\beta_h^M = 0.05$, and $\beta_c^M = 1$.

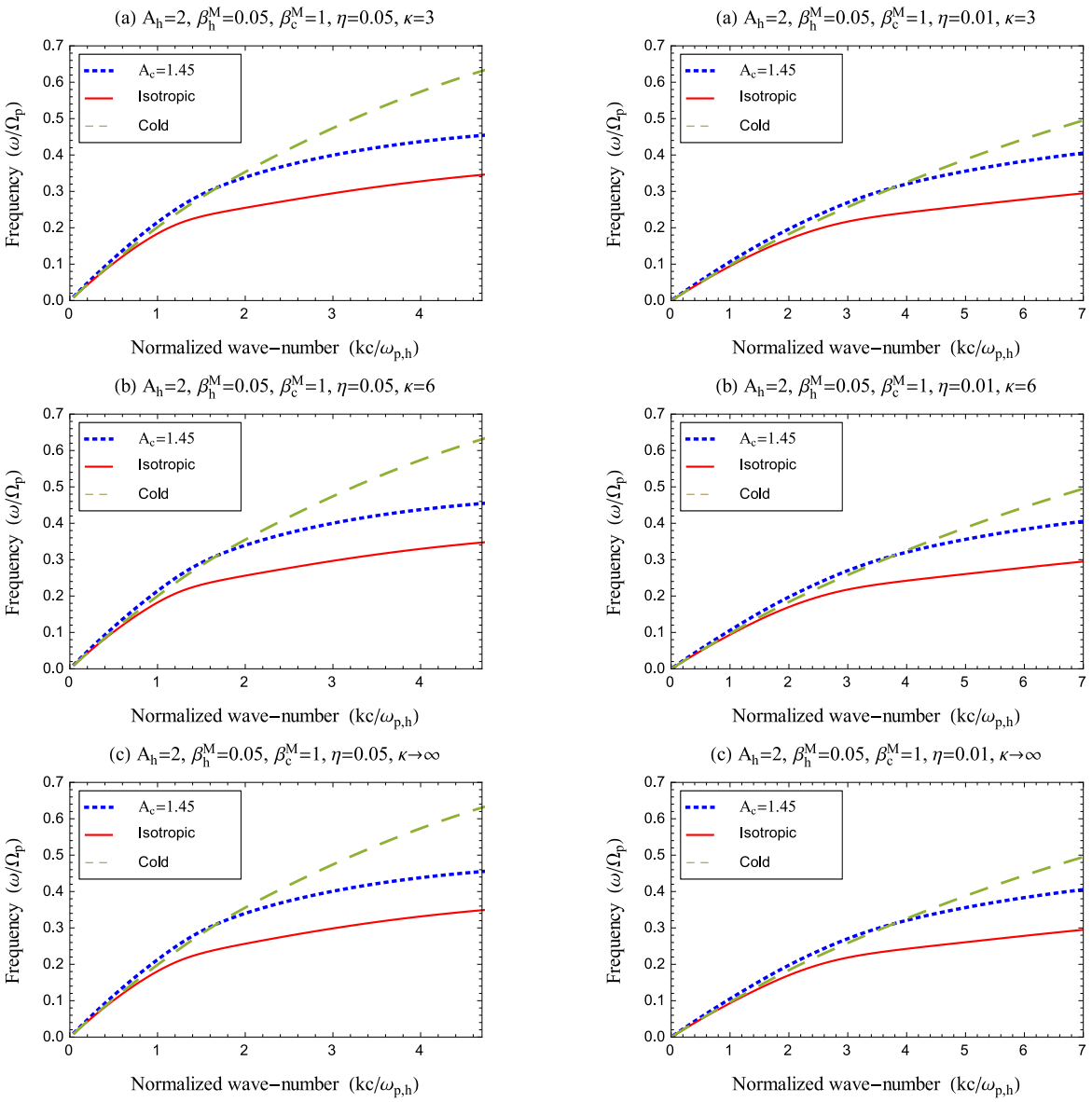

Figure 2. The wave-frequency of the unstable EMIC modes in Figure 1.

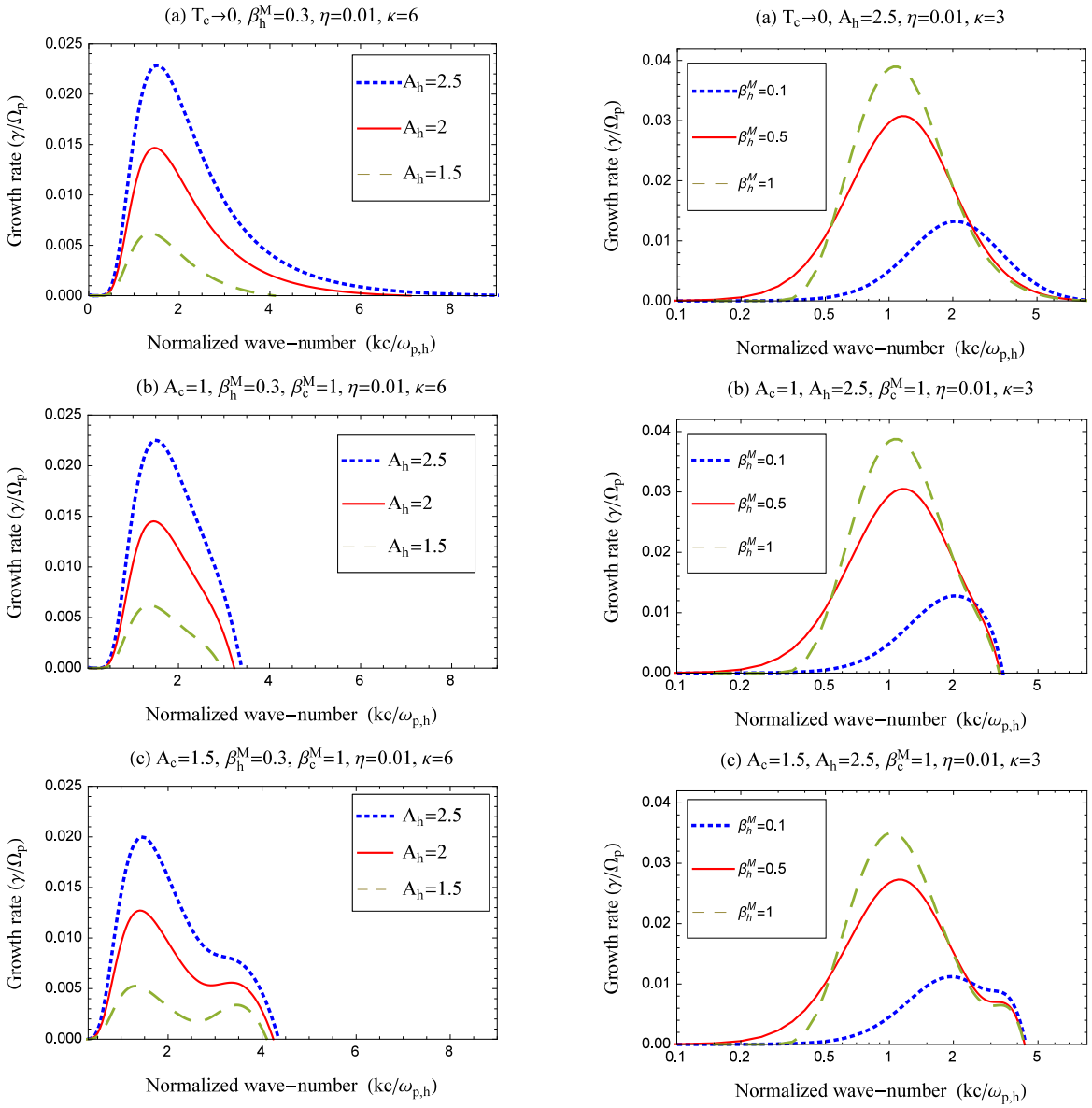

Figure 3. Effects of the halo anisotropy $A_h = 1.5, 2, 2.5$ (left panels) and the halo plasma beta $\beta_h^M = 0.1, 0.5, 1$ (right panels) on the growth rates of the EMIC instability. The plasma parameters and models considered for the core are explicitly given in each panel.

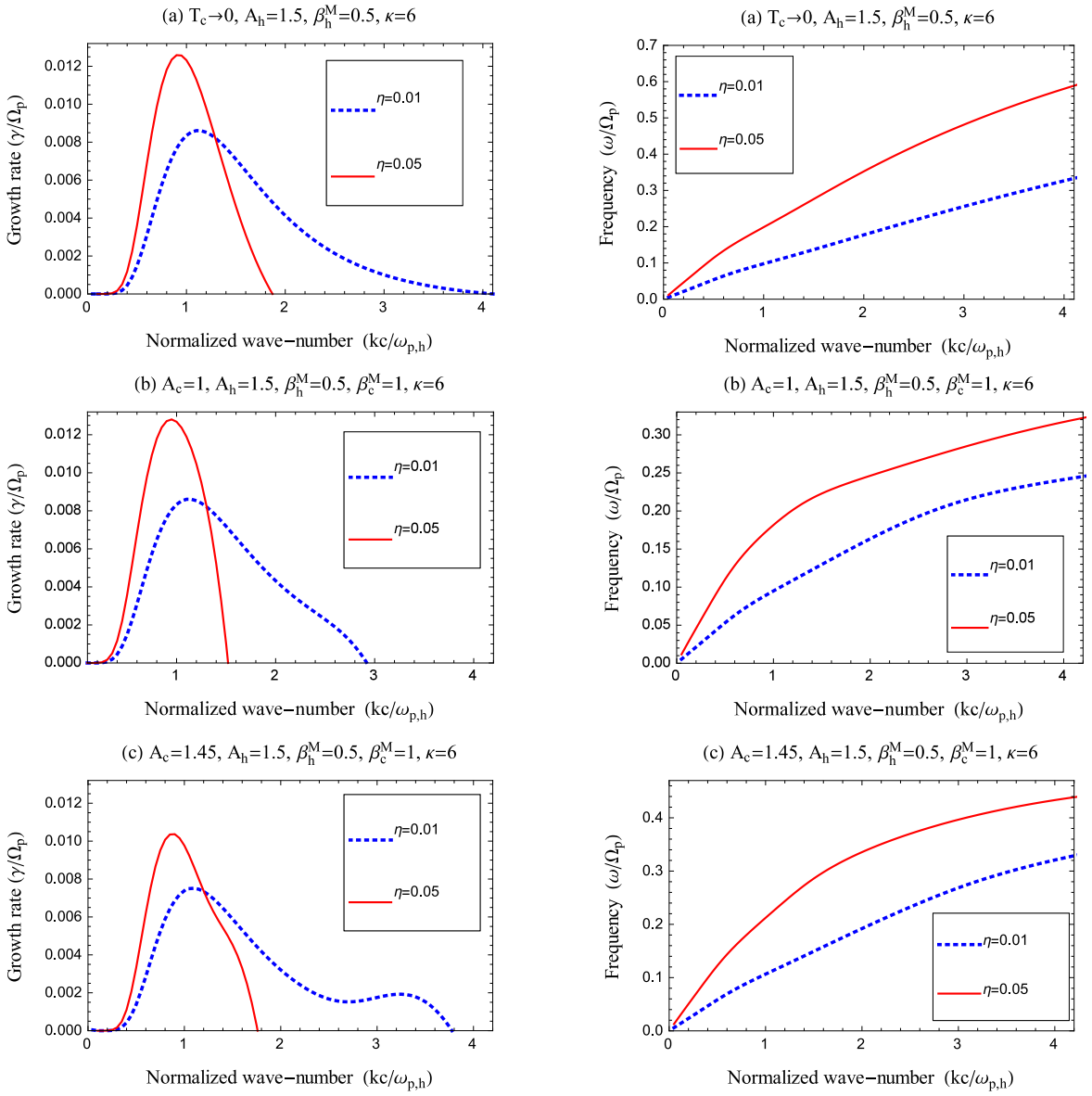

Figure 4. Effects of the halo-core density ratio η =0.05, and 0.01 on the growth rates and wave-frequencies of the EMIC instability. The plasma parameters and models considered for the core are explicitly given in each panel.

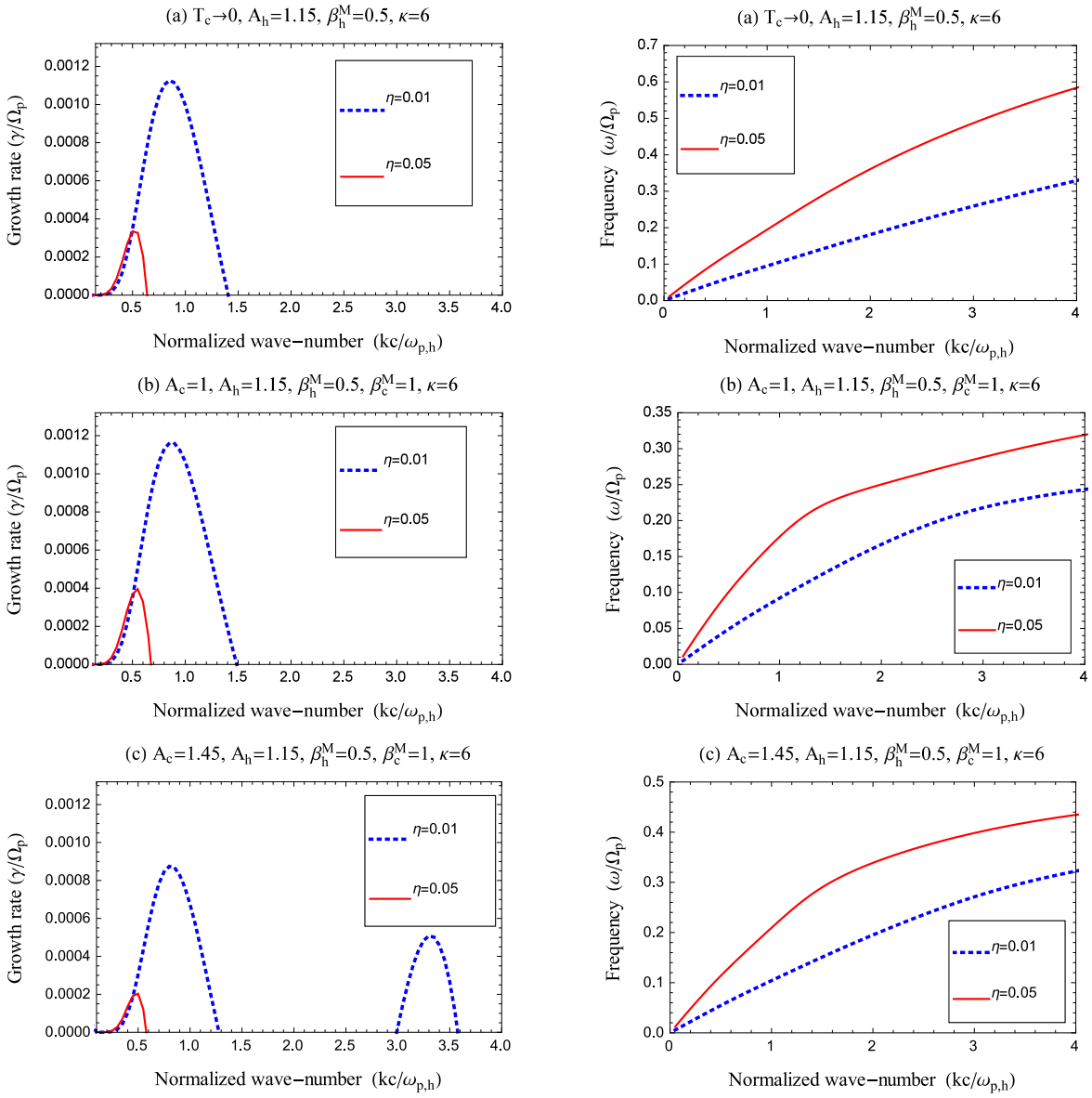

Figure 5. The same as in Figure 4 but for a lower anisotropy of the halo component $A_h = 1.15$.

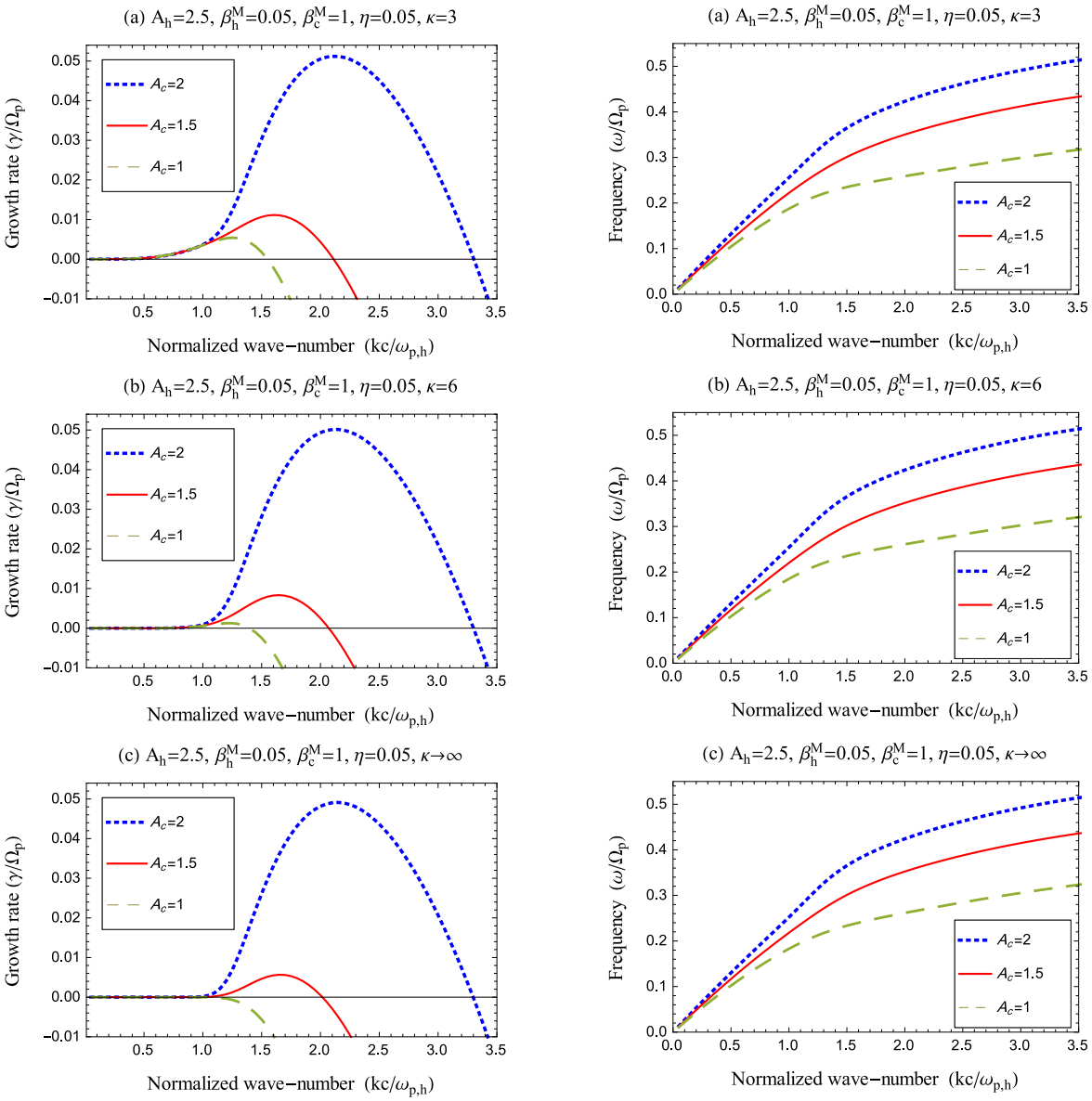

Figure 6. Effects of the anisotropic core $A_c = 2, 1.5, 1$ on the growth rate and the wave-frequency of the EMIC instability. The plasma parameters and models considered for the core and halo components are explicitly given in each panel.

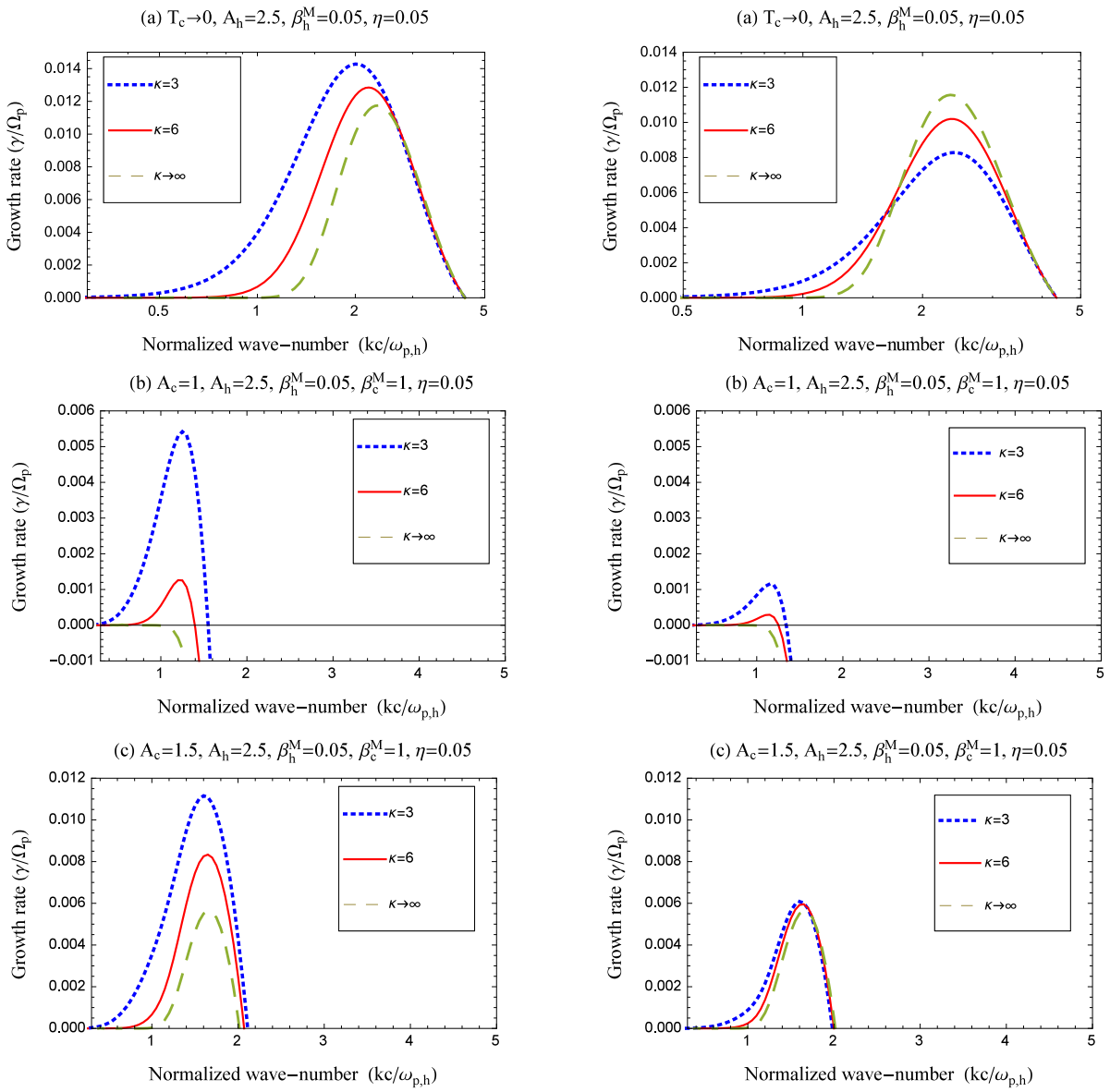

Figure 7. Growth-rates of the EMIC instability: a comparison between the two Kappa approaches with κ-dependent temperature (left) and κ-independent temperature (right). The plasma parameters and models considered for the core are explicitly given in each panel.

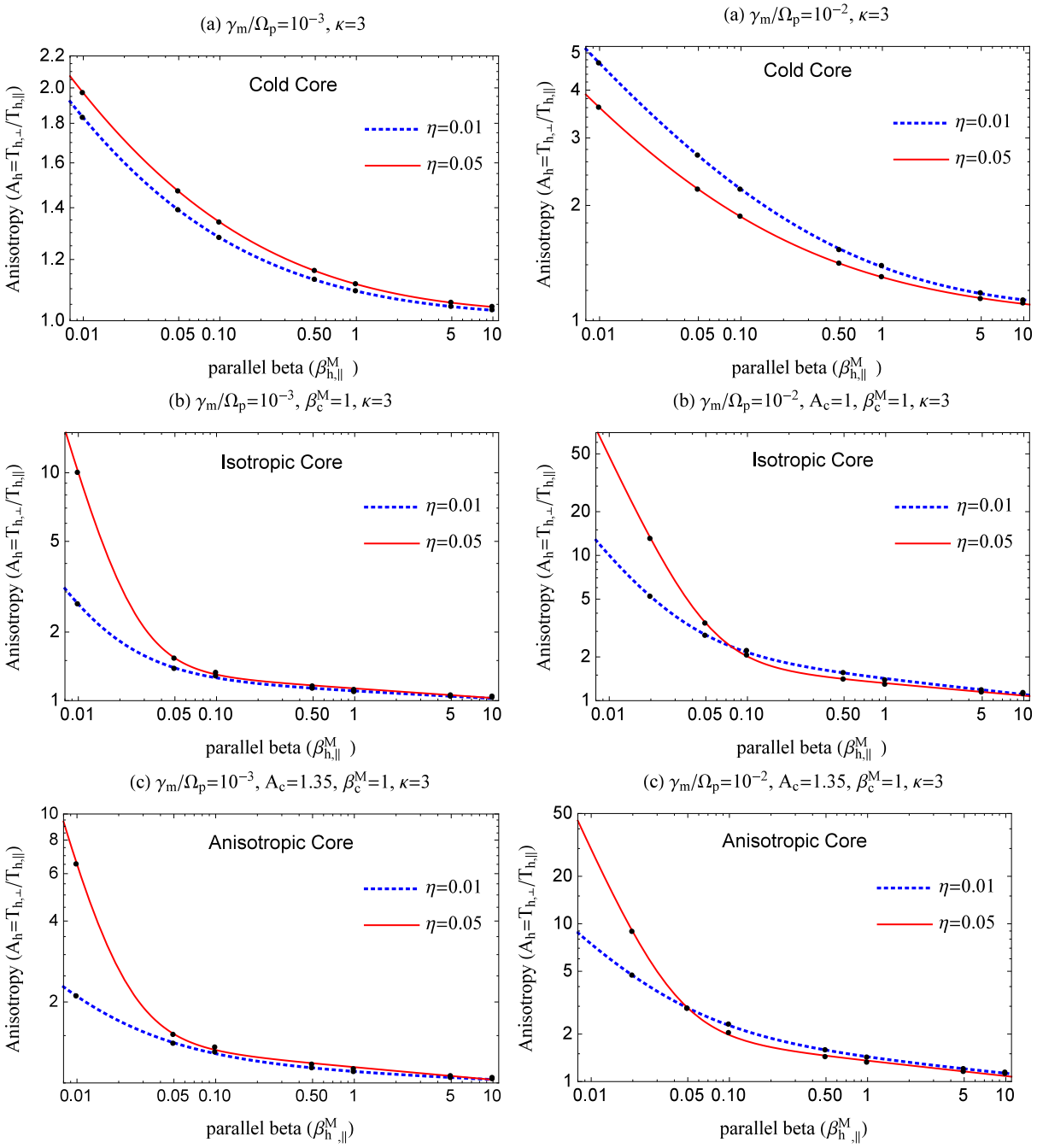

Figure 8. Effects of the halo-core density ratio $\eta = 0.05$, 0.01 on the EMIC thresholds $\gamma = 10^{-3}\Omega_p$ (left) and $\gamma = 10^{-2}\Omega_p$ (right). The plasma parameters and models considered for the core are explicitly given in each panel.

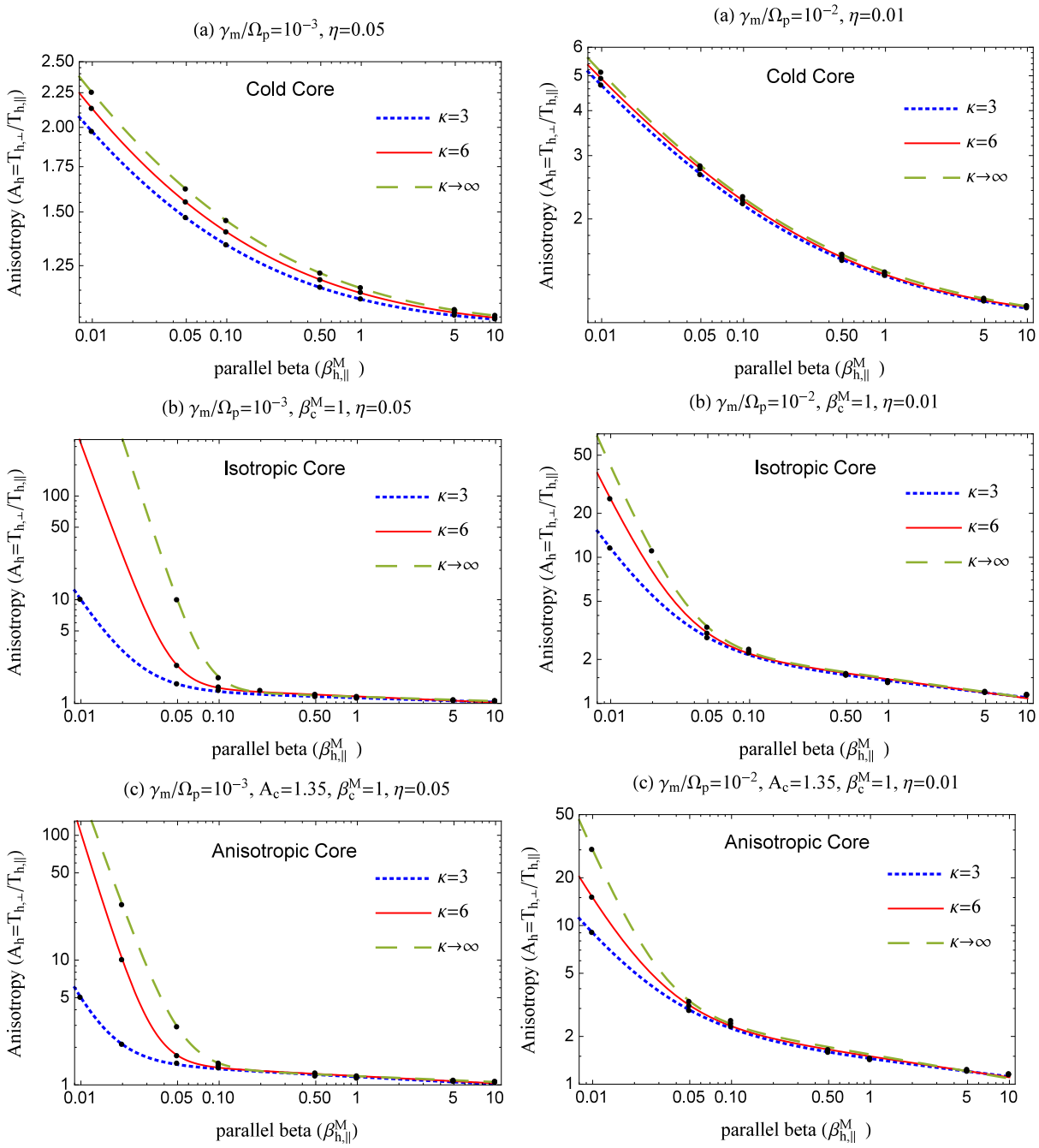

Figure 9. Effects of the power-index $\kappa = 3, 6, \infty$ on the EMIC thresholds $\gamma = 10^{-3}\Omega_p$ (left) with $\eta = 0.05$ and $\gamma = 10^{-2}\Omega_p$ (right) with $\eta = 0.01$. The plasma parameters and models considered for the core are explicitly given in each panel.

Table 1. Fitting parameters for thresholds $\gamma_{\rm m}/\Omega_p = 10^{-3}$ in Fig. 8

Model	η	a	b	c	d
Cold	0.01	0.094	0.472	1	0
	0.05	0.118	0.456	1	0
Iso.	0.01	0.0121	1.223	1.402	0.104
	0.05	0.0028	1.957	1.315	0.084
Aniso.	0.01	0.0461	0.876	1.372	0.087
	0.05	0.0021	1.894	1.353	0.096

Table 2. Fitting parameters for thresholds $\gamma_{\rm m}/\Omega_p = 10^{-2}$ in Fig. 8

Model	η	a	b	c	d
Cold	0.01	0.390	0.488	1	0
	0.05	0.292	0.473	1	0
Iso.	0.01	0.388	0.480	0.0002	2.052
	0.05	0.287	0.417	0.0065	1.789
Aniso.	0.01	0.419	0.478	0.0005	1.632
	0.05	0.318	0.450	0.0016	1.944

Table 3. Fitting parameters for thresholds $\gamma_{\rm m}/\Omega_p = 10^{-3}$ with $\eta = 0.05$ in Fig. 9

model	κ	a	b	c	d
Cold	3	0.118	0.456	1	0
	6	0.140	0.452	1	0
	∞	0.162	0.443	1	0
Iso.	3	0.00031	2.148	1.131	0.041
	6	0.00001	3.543	1.162	0.054
	∞	0.00003	4.044	1.160	0.043
Aniso.	3	0.00004	2.373	1.159	0.0595
	6	5×10^{-6}	3.532	1.176	0.058
	∞	0.00012	3.040	1.175	0.047

Table 4. Fitting parameters for thresholds $\gamma_{\rm m}/\Omega_p = 10^{-2}$ with $\eta = 0.01$ in Fig. 9

Model	κ	a	b	c	d
Cold	3	0.380	0.493	1	0.0
	6	0.399	0.494	1	0.0
	∞	0.409	0.499	1	0.0
Iso.	3	0.0069	1.370	1.419	1.370
	6	0.0014	1.887	1.461	0.130
	∞	0.0010	2.076	1.481	0.132
Aniso.	3	0.0188	1.091	1.424	0.106
	6	0.0052	1.469	1.489	0.129
	∞	0.0011	1.945	1.536	0.150